Optica Applicata, Vol. XXXIX, No. 1, 2009

Investigation of highly sensitive surface plasmon resonance biosensors with Au nanoparticles embedded dielectric film using rigorous coupled wave analysis

BIN WU*, QING-KANG WANG

National Key Laboratory of Micro/Nano Fabrication Technology, Key Laboratory for Thin Film and Microfabrication Technology of Ministry of Education, Research Institute of Micro/Nano Science and Technology, Shanghai Jiao Tong University, Shanghai, 200240, China

*Corresponding author: binwu@sjtu.edu.cn

The detection performance of conventional surface plasmon resonance (SPR) biosensors is limited by its own mechanism. Recently, novel highly sensitive SPR biosensors with Au nanoparticles enhancement are proposed to detect the interaction of small molecules in low concentrations. In this study, the effect of Au nanoparticles enhancement is firstly calculated by using the Maxwell–Garnett effective medium theory (EMT). Then, the influence of different structural parameters of nanoparticles embedded film on the performance is thoroughly investigated by the rigorous coupled wave analysis (RCWA). Electric field distributions in the nanoparticles embedded film are also given. The results strongly indicate that the sensitivity improvement can be achieved by adding a nanoparticle embedded film with optimal structural parameters. The simulation method of RCWA is also proved to be a powerful tool to optimize nanoparticles embedded film based biosensor.

Keywords: surface plasmon resonance biosensor, nanoparticles enhancement, effective medium theory (EMT), rigorous coupled wave analysis (RCWA).

1. Introduction

The surface plasmon wave (SPW) is free charge oscillation which occurs at the interface between dielectric and metallic medium. The incidence of light on the SPW causes excitation of the plasmon wave. When the momentum of the SPW matches that of the incident light, the so-called surface plasmon resonance (SPR) phenomenon takes place [1, 2]. It has been found that this wave-matching condition is very easily disrupted by even very tiny changes in the interface conditions. Hence, if the frequency is fixed, the SPR phenomenon not only permits the precise measurement of changes in the refractive index or thickness of the medium adjacent to the metal film, but also

enables changes in the adsorption layer on the metal surface to be detected. Consequently, various SPR biosensors have been developed in which the attenuated total reflection (ATR) method is functionalized by means of an immobilized surface on a metal sensing surface. These devices provide powerful tools for the real time investigation of biomolecular interaction analysis (BIA), and have the advantage that prior labeling of the analytes is unnecessary [3, 4]. SPR biosensors have been widely applied in a diverse range of fields, including molecular recognition, and disease immunoassays. However, their sensitivity is not high enough for some applications, such as sensing of aerosol or gas-phase release of toxins.

In order to overcome the sensitivity limitation, nanoparticle-based SPR biosensors have drawn tremendous interest in recent years, since it has been empirically shown that applying nanoparticles may significantly enhance their sensitivity [4–10]. In a conventional SPR biosensor using an attenuated total reflection scheme, the performance of the biosensor is determined by the surface plasmon polaritons (SPPs) excited on a thin metal film and propagating along the surface. However, the use of noble metal nanostructures allows strong optical coupling of incident light to resonances, the so-called localized surface plasmons (LSPs), which are collective electron oscillations localized in the metallic nanostructure. Various interactions between LSPs, SPPs, and binding biomaterial in the presence of nanostructures can lead to different resonance properties with an additional shift of resonance angle, resulting in enhanced sensitivity of a SPR biosensor.

In this paper, the effect of Au nanoparticles enhancement is firstly calculated in a conventional way using Maxwell–Garnett effective medium theory (EMT). Then, the influence of different structural parameters of nanoparticles embedded film on the performance is investigated by the rigorous coupled wave analysis (RCWA). Electric field distributions in the nanoparticles embedded film are also given to directly explain the performance difference for various structural parameters. We are particularly interested in the impact of geometrical parameters on the sensitivity enhancement in a SPR biosensor with nanoparticles embedded film, which is expressed by the shift of the resonance angle.

2. Numerical model

A schematic diagram of nanoparticles embedded film based SPR biosensor model is shown in Fig. 1, where spherical Au nanoparticles are represented as a one-dimensional array in a thin SiO_2 dielectric film, oriented along the x-axis. The SiO_2 film which contains Au nanoparticles is set on a gold layer. In the diagram, h, D and Λ represent the thickness of the gold film, the diameter of a nanoparticle and the period of the nanoparticle array, respectively. In this paper, the thickness of SiO_2 film is equal to the diameter of the nanoparticle, and the thickness of the flat Au film h is fixed on 30 nm.

The antibody analyte binding is modeled with a 1 nm thick self-assembled monolayer (SAM) that is supported by the thin gold film [11]. The complex indices

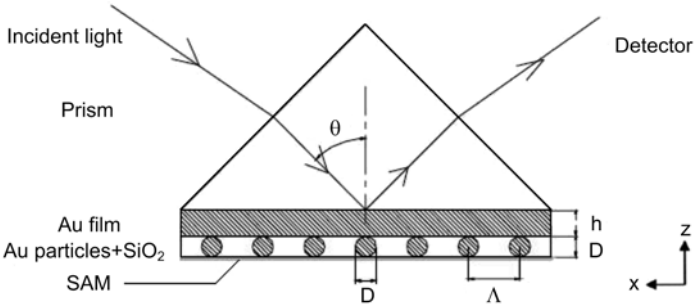

Fig. 1. Schematics of nanoparticles embedded film based SPR biosensor (*h* – gold layer thickness, *D* – nanoparticle diameter, *Λ* – nanoparticles period).

of refraction of the BK7 glass prism substrate, the SiO_2 dielectric film and Au were determined respectively as 1.719, 1.5, and 0.18 + 3.0*i* at $\lambda = 633$ nm [12]. In our study, we assumed SAM which has refractive index of 1.526. The SAM is extremely thin compared with the wavelength, so that the layer is essentially a lossless dielectric, and its extinction coefficient was thus ignored. The model in Fig. 1 assumes an illumination with a TM-polarized monochromatic plane wave at a fixed wavelength $\lambda = 633$ nm as the incidence angle θ is scanned with an angular resolution of 0.01°.

3. Results and discussions

As a quantitative measure of the sensitivity improvement, we introduce an angle shift enhancement factor (AS-EF) to represent the impact of Au nanoparticles embedded film on the SPR sensitivity in reference to a conventional SPR biosensor without nanoparticles embedded film as:

$$\text{AS-EF} = \left| \frac{\Delta\theta_{\text{NPSPR}}}{\Delta\theta_{\text{SPR}}} \right| = \left| \frac{\theta_{\text{NPSPR}}(\text{analyte}) - \theta_{\text{NPSPR}}(\text{noanalyte})}{\theta_{\text{SPR}}(\text{analyte}) - \theta_{\text{SPR}}(\text{noanalyte})} \right| \tag{1}$$

where $\Delta\theta$ is the difference between the plasmon resonance angles with and without analytes, and the subscripts NPSPR and SPR represent a nanoparticle enhanced SPR configuration and a conventional SPR scheme, respectively [11].

Figure 2 shows the SPR curves of nanoparticles embedded film based biosensor and conventional SPR biosensor. For the conventional SPR biosensor, the resonance angle shift is 0.09°, and that for the nanoparticles enhancement biosensor is 0.42°. In Figure 2, the AS-EF is calculated to be 4.67 and the width of the SPR curves is also broadened at the same time.

In the following, the profile effect of the structural parameters on the performance of the nanoparticles embedded film based biosensor is discussed. For the sake of convenience, the value of $\Delta\theta_{\text{SPR}}$ is fixed at 0.09°, which corresponds to the case of conventional SPR biosensor with 30 nm Au film.

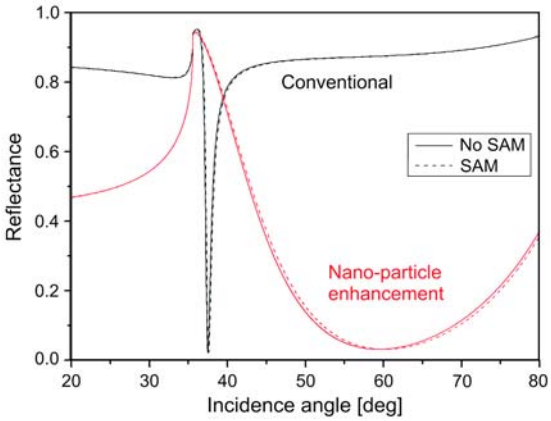

Fig. 2. SPR curves of nanoparticles embedded film based SPR biosensor and conventional SPR biosensor. For the conventional biosensor h = 45 nm, D = 0 nm; For the nanoparticles embedded film based biosensor, h = 30 nm, D = 15 nm, Λ = 40 nm.

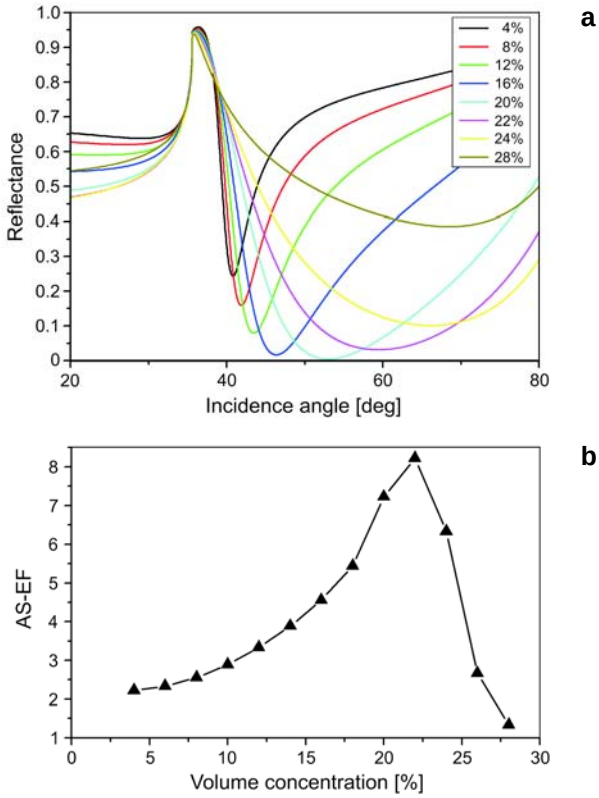

Fig. 3. Plots of SPR curves (**a**) and AS-EF values (**b**) for different Au nanoparticle volume concentrations based on Maxwell–Garnett EMT. The VF of the added metal varied from 4% to 28%.

In order to get the absorption spectrum of nanoparticles embedded film based SPR biosensor through simple Fresnel equations, the Maxwell–Garnett effective medium theory (EMT) model can be used, and has been employed in several papers [9, 10]. Prior to adopting this model, an assumption is made that the metal nanoparticles and the dielectric material are distributed homogeneously throughout the dielectric film or solution. According to the Maxwell–Garnett formula [13], the equivalent dielectric constant ε_{eff} is given explicitly by [14, 15]:

$$\varepsilon_{\text{eff}} = \varepsilon_d \frac{\varepsilon_m(1+2\phi)+2\varepsilon_d(1-\phi)}{\varepsilon_m(1-\phi)+\varepsilon_d(2+\phi)} \tag{2}$$

where ε_d and ε_m are the dielectric constants of the dielectric material and the added metal particles, respectively, and ϕ are the volume concentration of the added metal. If this model is to yield accurate predictions when adopted to evaluate the dielectric constant of films containing metal nanoparticles, it is necessary that the volume fraction (VF) of the added metal be smaller than 1/3. Furthermore, the size of metal nanoparticle should be much smaller than the wavelength of the incident light.

Having established the dielectric constants of the different layers, the Fresnel equations are employed to specify the reflectivity spectrum. Figure 3**a** shows the SPR curves for different Au nanoparticle volume concentrations based on the Maxwell–Garnett EMT as a function of the incident angle, when the VF is smaller than 1/3. Compared to conventional SPR biosensors, SPW excitation in the proposed SPR biosensor can be prompted by photons which are incident over a wider incident angle, because the momentum of the incident photons readily causes LSPs of the particles. In Figure 3**a**, it is obvious that the width of the curve becomes broader while the VF increases. However, the changing of sensitivity does not accord with this trend. Figure 3**b** shows the sensitivity curve as different VF, using the concept of AS-EF. When VF is 4%, the AS-EF is smallest, and then, it increases continuously and achieves the peak as volume fraction of 22%. Subsequently, the value of AS-EF decreases instead. It is clear, therefore, that achieving the optimal parameters of the Au nanoparticles embedded film is a crucial concern to form the high sensitivity SPR biosensors.

To study how the parameters of the Au nanoparticles embedded film influence the sensitivity of the SPR biosensor, the well-established RCWA [16, 17] is used in the following. The applicability of such a classical approach to metallic structure on a nanometer scale has been the topic of other studies [18, 19]. Convergence in RCWA can be achieved by including a sufficient number of space harmonics for the calculation of metallic surface relief structures even with rapidly varying fields in space. Comparing with the EMT, RCWA has the advantage to solve complicated structures in detail with no VF confine (for Maxwell–Garnett EMT, the confine is 1/3 volume fraction). It also can be utilized to produce approximate distribution of electromagnetic field intensity, as finite-difference time-domain (FDTD) method does.

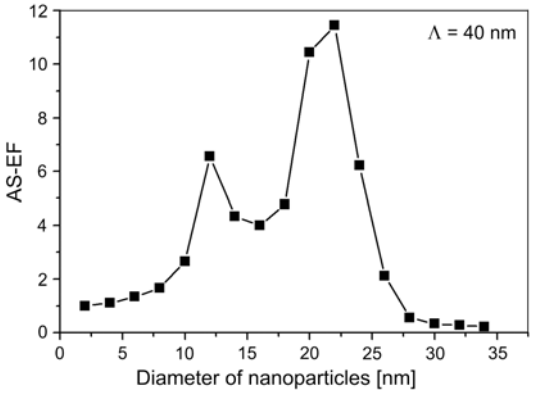

Fig. 4. Plots of AS-EF values for different Au nanoparticle diameters with fixed period. (The value of D varied from 4 nm to 34 nm with Λ fixed at 40 nm.)

Firstly, the influence of the nanoparticle diameter with fixed period is investigated. Figure 4 presents the plots of AS-EF values for different diameters. The value of D varied from 4 nm to 34 nm with Λ fixed at 40 nm. From Figure 4, the value of AS-EF increases as the nanoparticle diameter enlarges until it reaches the peak position, and then decreases. The highest peak AS-EF is 11.44 as diameter at 22 nm and the two lowest AS-EF values at sides are 1.01 at 2 nm and 0.22 at 34 nm, respectively.

The phenomenon shown in Fig. 4 can be interpreted in a simple way. When the diameter is too small, the Au nanoparticles embedded film is very thin and the nanoparticle VF of the film is very low. So the effect of localized surface plasmon resonance (LSPR) almost can be ignored. The biosensor in this case is basically equal to a conventional SPR biosensor and its sensitivity is close to conventional one. When the diameter is too large, the ultra-thick Au nanoparticles embedded film and the ultra--high VF make too strong absorption for light whose small amount of energy can be reflected. The biosensor in this case has no function to sensing and its sensitivity is close to zero. So, only an appropriate parameter can bring high sensitivity, just as the peak in Fig. 4. Another important phenomenon in Fig. 4 is that two peaks exist in it. The high one corresponds to the diameter of 22 nm while the low one refers to the diameter of 12 nm. This can be explained by two different resonance mechanisms in these two cases, which will be discussed in the following part. We also notice that when the diameter is 12 nm with fixed 40 nm period, the corresponding VF is 22%. This peak is completely in accord with the EMT results in Fig. 3**b**. Of course, the high peak in Fig. 4 with VF of 43% cannot be validated by EMT.

To clearly show the impact of nanoparticle diameter on sensitivity, the spatial distribution of magnetic field intensity $|H_y|$ is displayed in Fig. 5, which is calculated by RCWA. There are three cases of the diameter: 10 nm, 22 nm and 34 nm. In Figure 5**a**, the nanoparticle is too small, therefore its small amount of LSPs energy is submerged by bulk SPPs which is produced by the flat Au film. In Figure 5**c**,

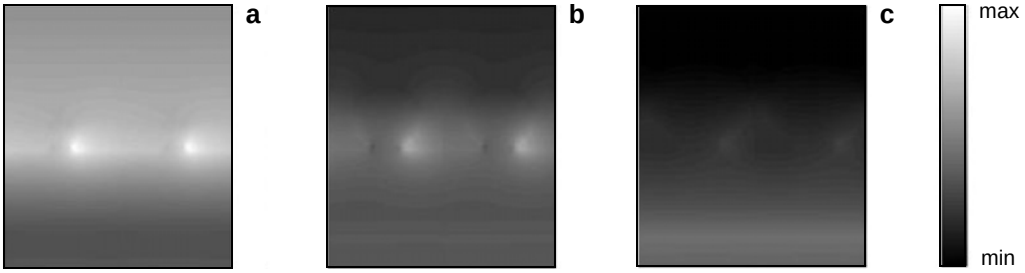

Fig. 5. Magnetic field intensity $|H_y|$ around the Au nanoparticles for different diameters with fixed period (we only give the field distribution in two periods); D = 10 nm (**a**), D = 22 nm (**b**), D = 34 nm (**c**).

the nanoparticle is too large and the whole film is too thick. The LSPs around the nanoparticle are very weak. So in the two cases above, there will not be effective sensitivity enhancement from the LSPs. But in Fig. 5**b**, the LSPs are strong and clear, and the bulk SPPs are relatively weak. Consequently, the LSPs enhancement will be impactful.

Then, the influence of the nanoparticle period with fixed diameter is studied. Figure 6 is the plot of AS-EF values for different periods. The value of Λ varied from 14 nm to 48 nm with D fixed at 12 nm. The most obvious character of this plot are the two AS-EF peaks. One peak corresponding to the period 18 nm is 9.22 and another peak corresponding to the period 40 nm is 6.56. This two-peak curve is similar with the curve shown in Fig. 4.

According to the theory of nanostructure LSPR enhancement [20], the LSPR is associated with two different modes of enhancement at a small or a large value of VF: single nanoparticle LSP excitation (low VF) and resonant coupling of LSPs through a nanogroove between nanoparticles (high VF). For Figures 4 and 6, the two AS-EF peaks reflect these two mechanisms, respectively. To validate this, the spatial

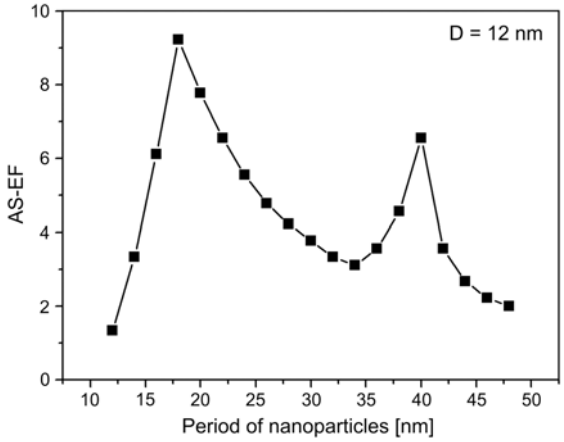

Fig. 6. Plots of AS-EF values for different Au nanoparticle periods with fixed diameter (the value of Λ varied from 14 nm to 48 nm with D fixed at 12 nm).

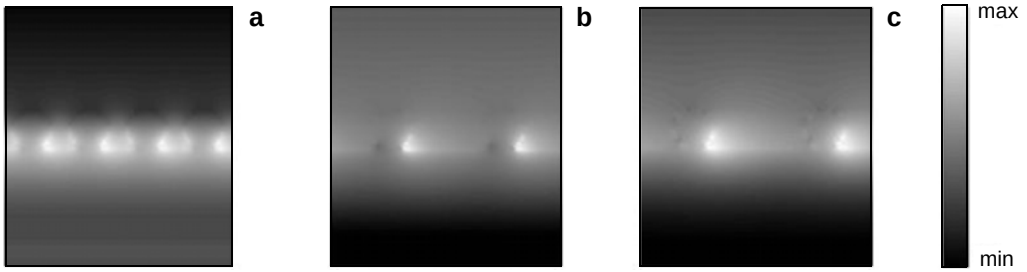

Fig. 7. Magnetic field intensity $|H_y|$ around the Au nanoparticles for different periods with fixed diameter (we only give the field distribution in a fixed range of 72 nm along the *x*-axes); Λ = 18 nm (**a**), Λ = 34 nm (**b**), Λ = 40 nm (**c**).

distribution of magnetic field intensity $|H_y|$, corresponding to two peaks (Λ = 18 nm and 40 nm) as shown in Fig. 6, and one vale (Λ = 34 nm), is displayed respectively in Fig. 7. In Figure 7**a**, the resonant coupling of LSPs through a nano-groove between nanoparticles is very strong. This is the main reason for the sensitivity enhancement in this case. In Figure 7**c**, the single nanoparticle LSP excitation is in dominance. Many LSPs points can be found round the nanoparticle. It is the main reason for the sensitivity enhancement in that case. But in Figure 7**b**, neither the resonant coupling of LSPs through a nanogroove between nanoparticles nor the single nanoparticle LSP excitation is strong. So its sensitivity enhancement is relatively weak. Combining Figs. 6 and 7, it can be also found that the LSP excitation associated with a nanogroove tends to have noticeably stronger sensitivity enhancement than that of a single nanoparticle.

Finally, the influence of different nanoparticle periods with fixed volume fraction is considered. The plot of AS-EF values for different periods is shown in Figure 8. The value of Λ varied from 20 nm to 90 nm with D/Λ fixed at 0.5. The value of AS-EF increases as the nanoparticle periods enlarge until it reaches the peak position

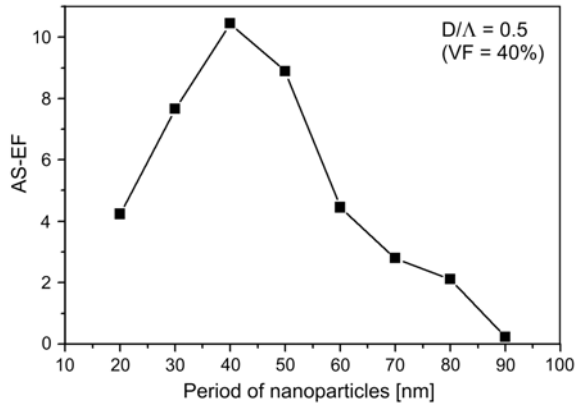

Fig. 8. Plots of AS-EF values for different Au nanoparticle periods with fixed volume fraction. (The value of Λ varied from 20 nm to 90 nm with D/Λ fixed at 0.5.)

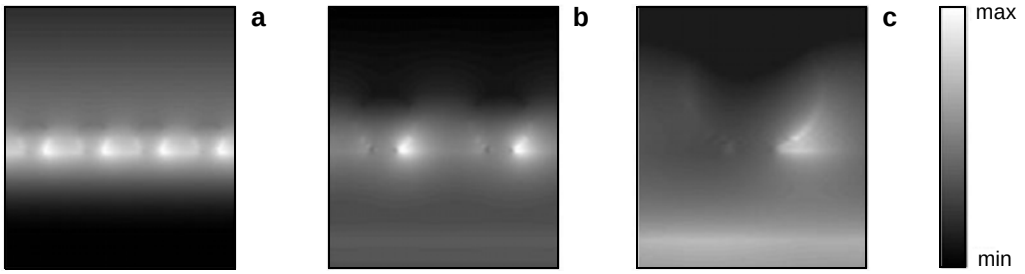

Fig. 9. Magnetic field intensity $|H_y|$ around the Au nanoparticles for different periods with fixed volume fraction (we only give the field distribution in a fixed range of 80 nm along the *x*-axes); Λ = 20 nm (**a**), Λ = 40 nm (**b**), Λ = 80nm (**c**).

and then decrease continuously. The peak AS-EF value corresponding to the period 40 nm is 10.44, while the lowest value for the period 90 nm is 0.22.

In fact, a narrow scale is propitious to generate strong LSPs in nanostructure. Therefore, a large period will in principle induce a low AS-EF value as a fixed wavelength of incident light. But on the other hand, too small nanoparticles cannot bring relative strong LSPs, while the thickness of a flat Au film and the wavelength of incident light are invariable, as discussed above. So, when D/Λ is fixed at 0.5, the value of AS-EF will reach an optimal peak point before it decreases with the period. To clearly show this process, the spatial distribution of magnetic field intensity $|H_y|$ is displayed in Fig. 9. There are three cases of the period: 20 nm, 40 nm and 80 nm. In Figure 9**a**, the distribution of LSPs is obvious, but the nanoparticle is so small that the LSPs energy and bulk SPPs are coupled. Then in Fig. 9**b**, the LSPs are clear and independent. It is the optimal case. As the period increases, in Fig. 9**c**, the scale of the whole structure is too large to generate strong LSPs. These results are very well in accord with Fig. 8.

According to our all simulated results, we have found that optimal structural parameters are necessary for the sensitivity improvement. A nanoparticle embedded film which is designed for resonant coupling between nanoparticles with small period is preferred. It has been also found that RCWA is more potent for the design of nanoparticle enhancement SPR biosensors in comparison with the conventional EMT analysis.

4. Conclusions

This work presents a comprehensive optimization analysis whereby one may gain quantitative insights regarding the dependence of sensitivity on structural parameters in nanoparticles embedded film based LSPR biosensor. More specifically, we have investigated the impact of design parameters on LSPs characteristics as well as a few unique features.

The traditional EMT is firstly used for an approximate analysis. And then the influence of different structural parameters on the performance is thoroughly

investigated by using RCWA. Electric field distributions around the nanograting are also given by RCWA to directly explain the performance difference for various structural parameters. These results indicate that nanoparticles of small period and optimal diameter show strong sensitivity enhancement, which is induced by LSPR. Also found is that the resonant coupling through a nanogroove and LSP excitation in a single nanoparticle are two main mechanisms for the LPSR enhancement. An optimum VF is located near high VF and low VF. In addition, the case of high VF induces larger LSPR enhancement than the low one.

The results strongly indicate that the possibility of sensitivity improvement by more than an order of magnitude in comparison with a conventional SPR structure can be achieved by adding a nanoparticle embedded film with optimal structural parameters. The simulation method of RCWA is also proved a powerful tool to optimize the nanoparticles embedded film based biosensor. Although the optimization was performed for a specific target analyte, we believe that the trends of stronger sensitivity enhancement for a nanogroove structure will remain valid for target materials of general interest. The difficulty is that the nanoparticles should be fabricated with precision to optimally tune both the period and the VF according with the optimal model. For realizing these optimal designs, actual fabrication technology should be improved.

Acknowledgments – This research was supported by a grant from the Nanotechnology Programs of Science and Technology Commission of Shanghai Municipality (No. 0652nm004).

References

[1] KRETSCHMANN E., RAETHER H., *Radiative decay of non-radiative surface plasmons excited by light*, Zeitschrift für Naturforschung A **23A**(12), 1968, pp. 2135–2136.

[2] OTTO A., *Excitation of nonradiative surface plasma waves in silver by the method of frustrated total reflection*, Zeitschrift für Physik A **216**(4), 1968, pp. 398–410.

[3] FLANAGAN M.T., PANTELL R.H., *Surface plasmon resonance and immunosensors*, Electronics Letters **20**(23), 1984, pp. 968–970.

[4] LUNDSTRÖM I., *Real-time biospecific interaction analysis*, Biosensors and Bioelectronics **9**(9–10), 1994, pp. 725–736.

[5] HE L., MUSICK M.D., NICEWARNER S.R., SALINAS F.G., BENKOVIC S.J., NATAN M.J., KEATING C.D., *Colloidal Au-enhanced surface plasmon resonance for ultrasensitive detection of DNA hybridization*, Journal of the American Chemical Society **122**(38), 2000, pp. 9071–9077.

[6] MALINSKY M.D., KELLY K.L., SCHATZ G.C., VAN DUYNE R.P., *Chain length dependence and sensing capabilities of the localized surface plasmon resonance of silver nanoparticles chemically modified with alkanethiol self-assembled monolayers*, Journal of the American Chemical Society **123**(7), 2001, pp. 1471–1482.

[7] HAES A.J., VAN DUYNE R.P., *A nanoscale optical biosensor: sensitivity and selectivity of an approach based on the localized surface plasmon resonance spectroscopy of triangular silver nanoparticles*, Journal of the American Chemical Society **124**(35), 2002, pp. 10596–10604.

[8] MCFARLAND A.D., VAN DUYNE R.P., *Single silver nanoparticles as real-time optical sensors with zeptomole sensitivity*, Nano Letters **3**(8), 2003, pp. 1057–1062.

[9] CHEN S.-J., CHIEN F.C., LIN G.Y., LEE K.C., *Enhancement of the resolution of surface plasmon resonance biosensors by control of the size and distribution of nanoparticles*, Optics Letters **29**(12), 2004, 1390–1392.

[10] HU W.P., CHEN S.J., HUANG K.T., HSU J.H., CHEN W.Y., CHANG G.L., LAI K.-A., *A novel ultrahigh-resolution surface plasmon resonance biosensor with an Au nanocluster-embedded dielectric film*, Biosensors and Bioelectronics **19**(11), 2004, pp. 1465–1471.

[11] KYUNG BYUN, SUNG KIM, DONGHYUN KIM, *Design study of highly sensitive nanowire-enhanced surface plasmon resonance biosensors using rigorous coupled wave analysis*, Optics Express **13**(10), 2005, pp. 3737–3742.

[12] PALIK E.D. [Ed.], *Handbook of Optical Constants of Solids*, Academic Press, Orlando 1985.

[13] MAXWELL-GARNETT J.C., *Colours in metal glasses and in metallic films*, Philosophical Transactions of the Royal Society of London, Series A **203**, 1904, pp. 385–420.

[14] LEUNG P.T., POLLARD-KNIGHT D., MALAN G.P., FINLAN M.F., *Modelling of particle-enhanced sensitivity of the surface-plasmon-resonance biosensor*, Sensors and Actuators B **22**(3), 1994, pp. 175–180.

[15] UNG T., LIZ-MARZAN L.M., MULVANEY P., *Gold nanoparticle thin films*, Colloids and Surfaces A **202**(2–3), 2002, pp. 119–126.

[16] MOHARAM M.G., GAYLORD T.K., *Diffraction analysis of dielectric surface-relief gratings*, Journal of the Optical Society of America **72**(10), 1982, pp. 1385–1392.

[17] MOHARAM M.G., GAYLORD T.K., *Rigorous coupled-wave analysis of metallic surface-relief gratings*, Journal of the Optical Society of America A **3**(11), 1986, pp. 1780–1787.

[18] KANAMORI Y., HANE K., SAI H., YUGAMI H., *100 nm period silicon antireflection structures fabricated using a porous alumina membrane mask*, Applied Physics Letters **78**(2), 2001, pp. 142–143.

[19] SUNTAK PARK, GWANSU LEE, SEOK-HO SONG, CHA-HWAN OH, PILL-SOO KIM, *Resonant coupling of surface plasmons to radiation modes by use of dielectric gratings*, Optics Letters **28**(20), 2003, pp. 1870–1872.

[20] KIM K, YOON S. J, KIM D., *Nanowire-based enhancement of localized surface plasmon resonance for highly sensitive detection: a theoretical study*, Optics Express **14**(25), 2006, pp. 12419–12431.

Received February 21, 2008
in revised form June 7, 2008